

SUPPORTING INFORMATION

Copper-based sorbent with oxygen-vacancy defect from mechanochemical reduction for carbon disulfide absorption

*Haipeng Chen,^{ab} Shixue Zhou,^{*ab} Zongying Han,^{a,c} Yaoyao Jiang,^d Hao Yu,^{ab} Xinpei Zhou,^a
Ruiqian Jiang,^a Xiaojing Liu^a and Xinyuan Li^a*

^aCollege of Chemical and Environmental Engineering, Shandong University of Science and Technology, Qingdao 266590, China

^bState Key Laboratory of Mining Disaster Prevention and Control Co-founded by Shandong Province and the Ministry of Science and Technology, Shandong University of Science and Technology, Qingdao 266590, China

^cUnion Research Center of Fuel Cell, School of Chemical and Environmental Engineering, China University of Mining and Technology, Beijing 100083, China

^dSinochem Hongrun Petrochemical Co., Ltd., New and High Technology Industry Development Zone, Weifang 261061, China

Corresponding author: Tel: +86 532 86057857. E-mail: zhoushixue66@163.com (S.X. Zhou)

Materials: CuO, Cu₂O, Cu and Mg were purchased from Tianjin Ruijinte Chemical Company, China, and used as received. MgO was purchased from Beijing Nachen Science & Technology Development Co., Ltd. Anthracite coal was purchased from Rujigou Mine, China. The anthracite has low volatile matter content (6.60 wt.%, air dry basis), low ash content (8.55 wt.%) and high fixed carbon content (83.00 wt.%).

Demineralization and carbonization of anthracite: Carbon additive from anthracite via demineralization and carbonization was used as milling aid. For demineralization, 10.0 g of anthracite and 12.0 g of NaOH were mixed in a stainless-steel vessel and heated at 400 °C for 1.5 h. After that, the mixture was cooled down to room temperature and rinsed with deionized water. Next, the anthracite was mixed with 120 mL of hydrochloric acid (20 wt%) and heated at 80 °C in water bath for 4.0 h. Then, the anthracite was rinsed with deionized water. For carbonization, the anthracite was charged into a crucible and carbonized at 900 °C for 1.0 h under argon atmosphere.

Weight ratio of CuO to Mg during ball milling is of critical importance for the composition of reduction product. XRD patterns of Cu-based sorbents from different ratios of CuO to Mg are shown in Figure S1. It is clear that when the addition of CuO decreases from 90 wt% to 75 wt%, the amount of Cu₂O decreases while that of Cu increases. With further decreasing CuO (e.g., CuO10Mg90), Mg, MgO and Cu phases will dominate in the sorbent, while Cu₂O is negligible. On the contrary, when excessive CuO is added (e.g., CuO95Mg5), CuO cannot be effectively reduced, resulting in the low generation of Cu₂O. Thus, the weight ratio of CuO to Mg for sorbent preparation should be around 9:1 to control the amount of Cu₂O in a high level.

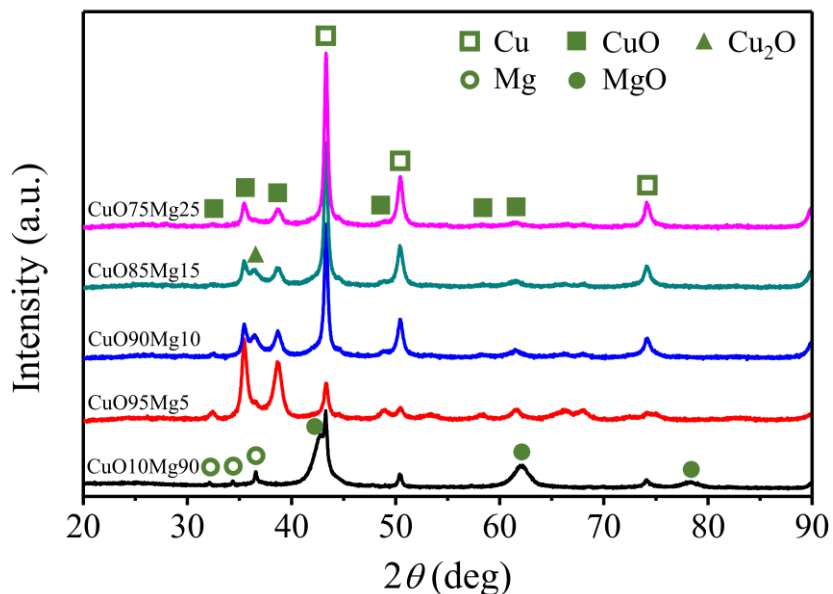


Figure S1. XRD patterns of Cu-based sorbents for 1.0 h of ball milling from different ratios of CuO to Mg. The samples are named as CuO_xMg_y for convenience, where *x* and *y* denote the composition of CuO and Mg in weight.

CuO and Cu₂O crystal cells were constructed with the lattice parameters from Rietveld refinement of XRD data. Their supercells were constructed with (2 × 2) (111) slabs of six atomic layers and vacuum space (20 Å) as periodic boundary conditions.

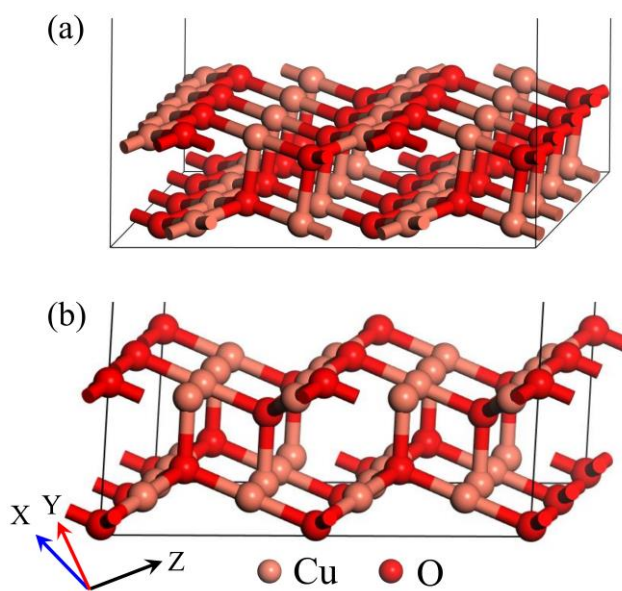


Figure S2. Supercells of CuO(111) (a) and Cu₂O(111) (b).

The S-doped ($2 \times 2 \times 2$) supercell was constructed from Cu_2O cell by substitution of 16.67% (atomic fraction) O atoms with S atoms. Thus, the sulfur concentration is 10.5 wt% in total, in consistent with the sulfur content from CS_2 absorption at 150 °C (10.7 wt%).

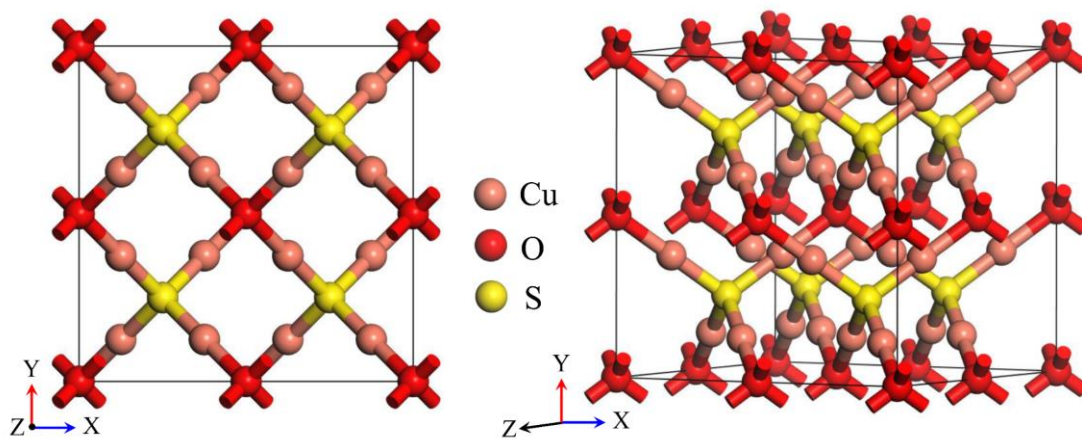


Figure S3. Supercell of the S-doped Cu_2O .

Figure S4 shows XRD patterns of CuO/carbon (9:1) mixture (a) and pure CuO (b) from 3.0 h of milling. From Figure S4, CuO cannot be reduced without Mg as reducing agent during ball milling, and carbon additive just plays a role of milling aid to increase the reduction efficiency by dispersing Mg and CuO particles.

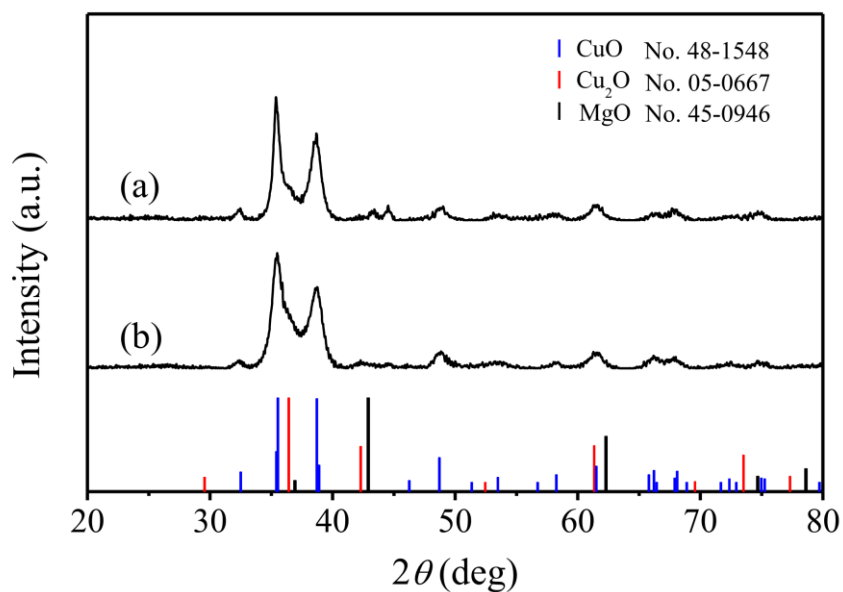


Figure S4. XRD patterns of CuO/carbon mixture (a) and pure CuO (b) from 3.0 h of milling.

For the material from before and after ball milling, they both exhibit a type IV isotherm, indicating the existence of macropores and mesopores. The specific surface areas are calculated to be $8.9 \text{ m}^2 \text{ g}^{-1}$ from ball milling and $11.9 \text{ m}^2 \text{ g}^{-1}$ without ball milling, by using the BET equation. The increase of specific surface area by ball milling is expected to improve the desulphurization activity of the sorbent.

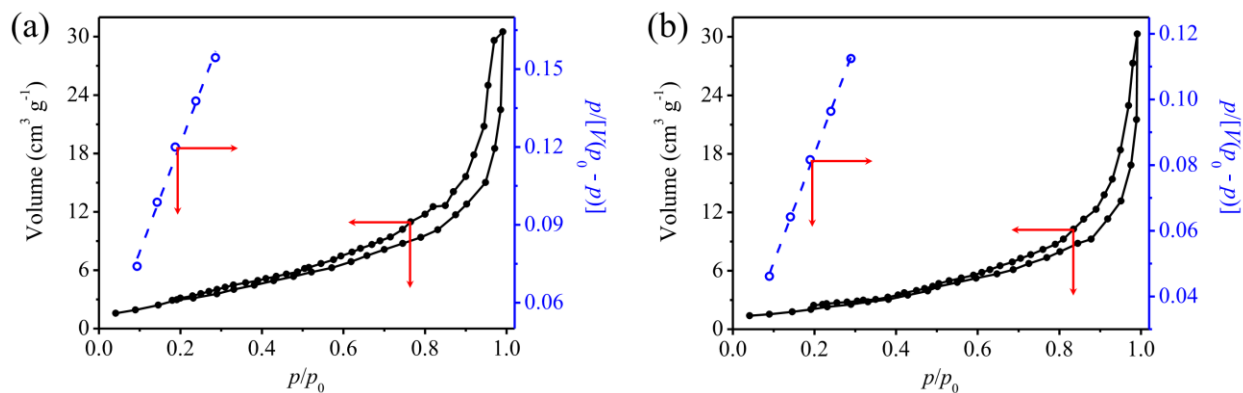


Figure S5. N_2 physisorption isotherms and plots of $p/[V \cdot (p_0 - p)]$ versus p/p_0 for the material before (a) and after (b) ball milling.

XRD patterns of MgO, Cu, Cu₂O and CuO without ball milling after CS₂ absorption at 150 °C for 4.0 h are shown Figure S6, in which there is no CuS or Cu₇2S₄ observed, indicating that raw MgO, Cu, Cu₂O and CuO cannot absorb CS₂ at such conditions.

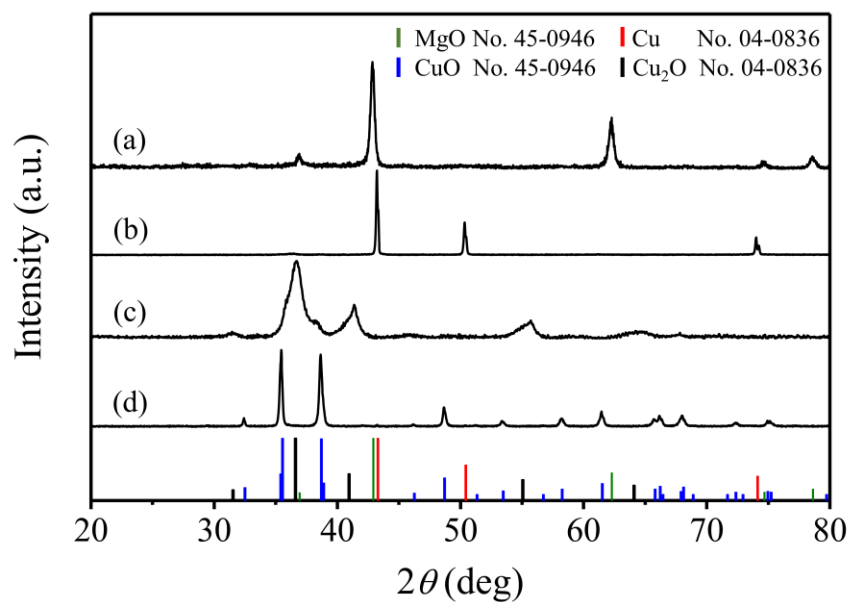


Figure S6. XRD patterns of MgO (a), Cu (b), Cu₂O (c) and CuO (d) (without ball milling) after CS₂ absorption at 150 °C for 4.0 h.

Breakthrough sulfur capacities of sorbents from 1.0, 2.0 and 3.0 h of milling are measured to be, respectively, 10.7 wt%, 6.8 wt% and 4.3 wt%. Three aspects, i.e., crystallite size, chemical surrounding of Cu surface, deposit carbon from reaction between Cu and CS₂, can affect the CS₂ absorption performance of Cu phase from CuO reduction. With the extension of milling time, the crystallite size of Cu grows up, and the coverage of MgO and deposit carbon on Cu surface increases, which are all unfavorable for the CS₂ absorption. Thus, the milling time of CuO should be controlled at around 1.0 h to keep the amount of Cu in a low level.

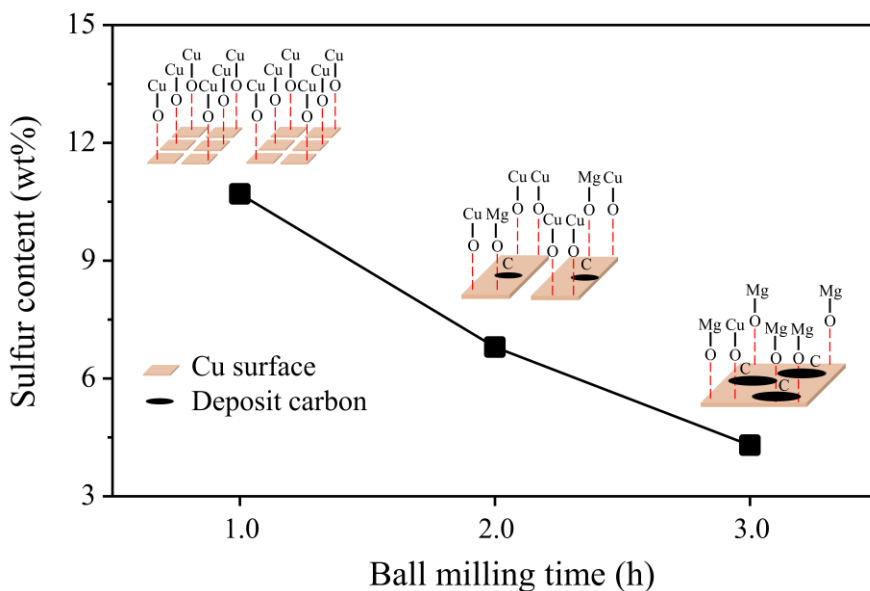


Figure S7. Sulfur capacities of sorbents from different milling time after CS₂ breakthrough at 150 °C, in which the inset is schematic illustration for chemical surrounding of Cu surface.

Coordination states of copper on CuO(111) and Cu₂O(111) can be changed by the O_{vac} defect. Figure S8 shows the coordination states of copper on clean (a, b) and O_{vac} defective (c, d) CuO(111) and Cu₂O(111). Table S1 shows the calculated surface energy of CuO(111) and Cu₂O(111).

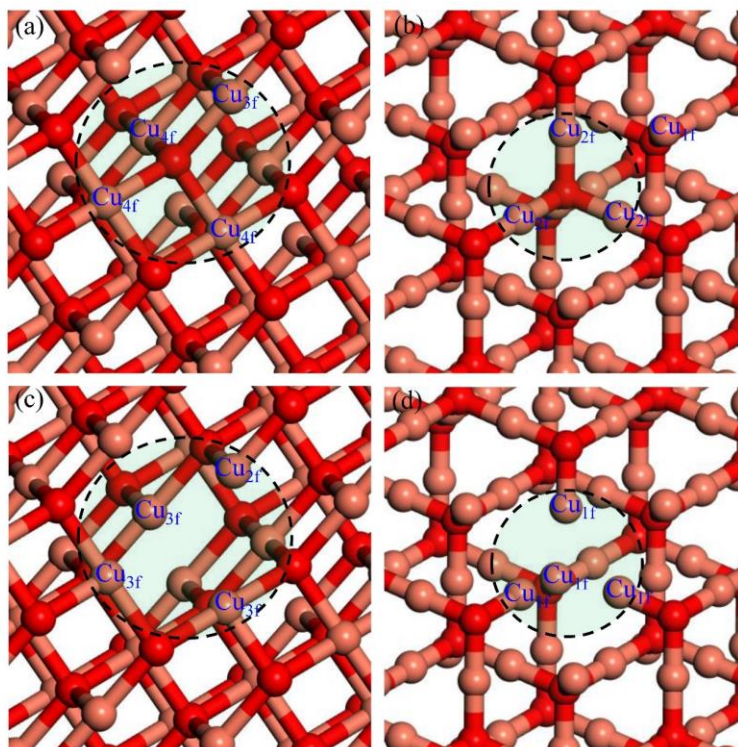


Figure S8. Coordination states of copper on clean (a, b) and O_{vac} defective (c, d) CuO(111) and Cu₂O(111). The orange and red spheres represent Cu and O atoms, respectively.

Table S1 Coordination of copper and surface energy of CuO(111) and Cu₂O(111).

Surfaces	Crystal inner coordination	Surface coordination	σ (eV nm ⁻²)
CuO(111)	4f (100%)	3f (50%) & 4f (50%)	1.41
Cu ₂ O(111)	2f (100%)	2f (75%) & 1f (25%)	2.13

After chemisorption, the C–S bond of CS₂ molecule stretches and the S-C-S bond angle decreases compared with that of typical CS₂ molecule ($L_{C-S} = 1.553 \text{ \AA}$, $\angle S-C-S = 180^\circ$). The chemisorption energy of CS₂ molecule increases due to the introduction of O_{vac} defect.

Table S2 Structural parameters and chemisorption energy of CS₂ molecule after chemisorption.

Surfaces	$L_{C-S}(\text{\AA})$	$\angle S-C-S$ ($^\circ$)	$E_{CS_2\text{-ads}}$ (kJ mol ⁻¹)
CuO(111) without O _{vac} defect	1.574	146.86	-70.42
Cu ₂ O(111) without O _{vac} defect	1.581	140.01	-92.66
CuO(111) with O _{vac} defect	1.577	143.60	-75.64
Cu ₂ O(111) with O _{vac} defect	1.584	178.96	-110.45